Hindawi
Advances in Civil Engineering
Volume 2022, Article ID 3687475, 10 pages
https://doi.org/10.1155/2022/3687475

Research Article

Experimental Study on a Low-Rise Shear Wall with the Built-In Shear Steel Plate

Xingyu Song,[1] **Lin Zhao**,[1] **Lingkun Chen**,[1,2] **Yuan Duan**,[3] **Yehao Jiang**,[4] **and Yuan Tian**[5]

[1]*College of Architectural Science and Engineering, Yangzhou University, Yangzhou 225000, China*
[2]*Department of Civil and Environmental Engineering, University of California, Los Angeles 90095, CA, USA*
[3]*Shanxi Institute of Chemical Engineering Design, Taiyuan 030000, China*
[4]*School of Civil Engineering, Yangzhou Polytechnic College, Yangzhou 225009, China*
[5]*Transportation Technology Development Promotion Center, China Academy of Transportation Sciences, Beijing 100029, China*

Correspondence should be addressed to Lingkun Chen; lkchen@yzu.edu.cn

Received 19 November 2021; Revised 27 May 2022; Accepted 13 June 2022; Published 11 July 2022

Academic Editor: Andreas Lampropoulos

In this paper, a new reinforcement scheme is proposed to improve the seismic performance of low-rise shear walls. The new system combines the advantages of slotted and composite shear walls to exhibit a high bearing capacity and good deformation performance. Two low-cycle repeated loading tests with different forms of shear walls were conducted to accurately understand its seismic performance. Seismic performance indexes, such as failure mode, bearing capacity, hysteresis curve, stiffness degradation, and energy dissipation capacity, of the new shear wall under the low-cycle reciprocating load were obtained to verify its reliability. The results show that the newly reinforced shear wall has two clear seismic defense lines. Its deformation and energy-dissipation capacities and lateral stiffness stability are greatly improved compared with traditional low-rise shear walls. Thus, the proposed method can provide a new means for enhancing the seismic performance of shear walls.

1. Introduction

Reinforced concrete shear walls, the prominent lateral force-resisting members used in high-rise structures, have high bearing capacity and stiffness. However, widespread seismic damage and experimental research [1–3] show that the low-rise shear walls with small aspect ratios (height to width ratios) and high axial compression ratios have poor ductility and energy dissipation capacity, which were seriously damaged during strong earthquakes. The failure process has the characteristics of brittle shear failure, which is not conducive to the seismic performance of the structure. Low-rise shear walls always exist in a multistory frame-shear wall at bottom story structures and high-rise large-space in basement structures. However, their ductility is poor and the number and thickness of the shear wall are restricted by architectural function. So it is urgent in the engineering field to develop a new kind of low-rise shear wall which has a better seismic behavior.

To improve the deformation capacity and seismic performance of shear walls, researchers have carried out many studies and proposed many improvement measures. Muto [4] studied the seismic performance and the force mechanism of shear walls with vertical slits, and the results show that the method of opening vertical slits can effectively improve the deformation performance of shear walls. Studies have shown that an appropriate slit setting can change the failure mode of the shear wall and effectively improve the energy dissipation capacity and ductility of low-rise shear walls [5, 6]. Other research studies have studied the seismic behavior of shear walls with diagonal reinforcement, and the results show that oblique reinforcement could improve the deformation capacity of the shear wall, slow down the stiffness degradation, and effectively avoid shear failure [7, 8]. Experimental research on shear walls with concealed bracings was also conducted, and the results show that owing to the existence of bracings, the cracks in the concrete were fully developed; the overall stiffness

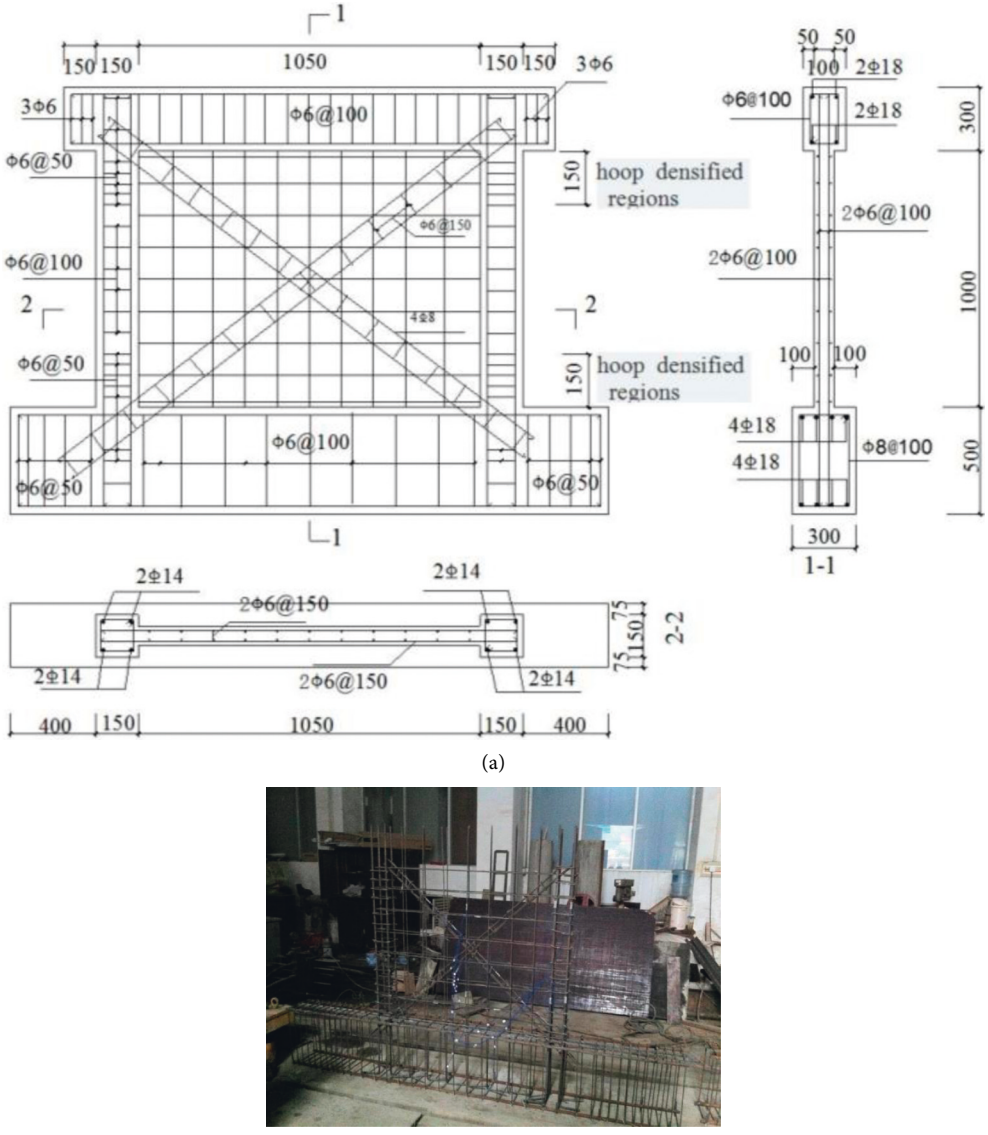

(a)

(b)

Figure 1: Reinforcement details and the actual model of HDLSW. (a) Reinforcement details of HDLSW. (b) Actual model of HDLSW.

decreased slowly throughout the test, which improved the seismic performance of the shear walls [9–11]. The seismic behavior of composite shear walls is studied by authors of reference [12, 13], and the test results indicate that the composite shear walls with embedded steel plate reinforcement can enhance the advantages of steel and concrete combination, improve the bearing capacity and lateral stiffness of the shear wall, and reduce the section area of the shear wall. Other scholars have obtained the contribution coefficients of different parts of the composite shear wall through a large number of numerical simulations [14–16].

However, existing research on improving the deformation performance of shear walls was focused on high aspect ratio walls. In contrast, walls with aspect ratios below 1.0 have received little attention. In fact, low-rise shear walls are more prone to brittle shear failure than high-rise shear walls during earthquakes. Opening vertical slits in the wall can effectively improve the ductility of a low-rise shear wall, but they will sacrifice the initial stiffness and bearing capacity of the shear wall. In this paper, a new slit shear wall with a built-in steel plate and concealed steel bracings has been brought forward. The experimental study on the seismic behavior of this new shear wall has been performed in this paper.

2. Experimental Program

2.1. Test Specimens. In this study, two low-rise shear walls with an aspect ratio of 0.74 were designed (HDLSW and HDNLSW). On both sides of the two shear walls are 150 mm × 150 mm frame columns, the wall height is 1000 mm, and the wallboard between the frame columns is 1050 mm wide and 100 mm thick. HDLSW is a low-rise shear wall with concealed steel bracings as a comparison

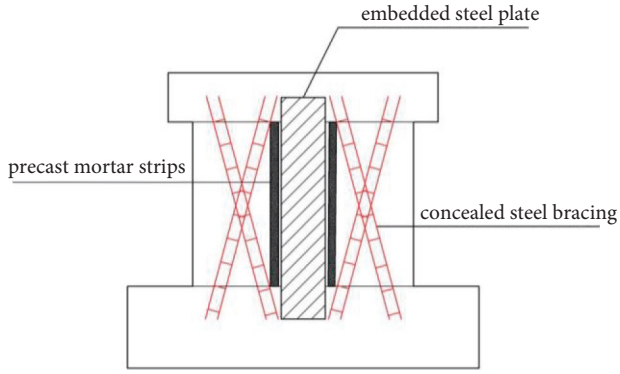

Figure 2: HDNLSW structure diagram.

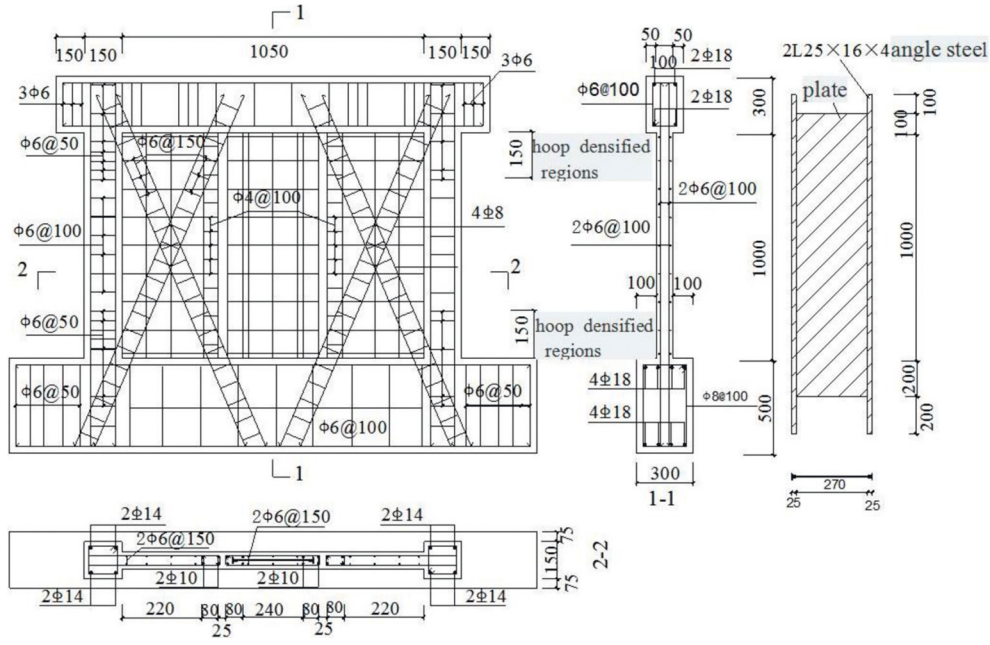

(a)

(b)

Figure 3: Reinforcement details and the actual model of HDNLSW. (a) Reinforcement details of HDNLSW. (b) Actual model of HDNLSW.

specimen, and the reinforcement details and the actual model are shown in Figure 1. HDNLSW is a slotted low-rise shear wall with a built-in steel plate proposed in this paper. The structural diagram is shown in Figure 2, and the reinforcement details and actual model are shown in Figure 3. The production process of HDNLSW mainly includes three steps. Firstly, two vertical slits were opened on the wallboard of the shear wall to divide the low-rise shear wall into three parts. Then, the concealed steel bracings were set on the wallboard on both sides, and the steel plate was embedded in

Table 1: Parameters of specimens.

Specimen	Span ratio	Net height of the wallboard (mm)	Net width of the wallboard (mm)	Frame column (mm)	Width of slit (mm)
HDLSW	0.74	1000	1050	150×150	—
HDNLSW	0.74	1000	1050	150×150	25

Table 2: Properties of reinforcing bars and the steel plate.

Specification	Yield strength (MPa)	Ultimate strength (MPa)	Elastic modulus (MPa)
Φ4	270	368	2.02×10^5
Φ6	458	542	2.01×10^5
Φ8	407	477	2.07×10^5
Φ10	416	461	2.03×10^5
Φ14	385	518	2.03×10^5
Φ18	380	527	2.01×10^5
Steel plate	289	415	1.98×10^5

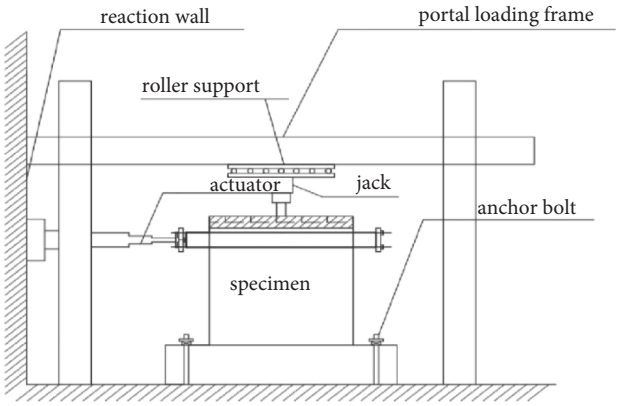

Figure 4: Test setup.

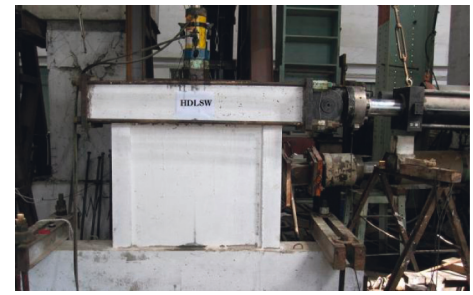

Figure 5: Loading site.

the wallboard between the vertical slits. Finally, the cement mortar block was placed at the slits, and then, the concrete was poured as a whole to form the shear wall. The size of the shear walls is summarized in Table 1.

2.2. Material Performance. The concrete cubic compressive strength f_{cu} was determined by the compression test on standard cubic samples (three $150\times150\times150$ mm cubes were used as test samples in each specimen). In the code for the design of concrete structures in China (GB50010-2010) [17], the average compressive strength of concrete f_c was taken $f_c = 0.76f_{cu}$. The f_c was tested to be equal to 34.1 MPa, and the elastic modulus of the concrete E_c was 3.06×104 MPa. Regarding the reinforcement, the average values of the yield strength $f_{y,m}$ and the tensile strength $f_{u,m}$ are shown in Table 2. It should be noted that all bars were hot-rolled plain steel bars except Φ4 mm bars, which were cold-rolled ribbed bars.

2.3. Test Apparatus and the Loading System. The dynamic and quasi-static tests were performed before and after loading to obtain each specimen's change in frequency and damping. Low cyclic reversed loading tests of two shear walls were carried out, and the test device is shown in Figure 4. During the test, the foundation beam was anchored to the test bench by using an anchor beam and an anchor bolt, and the loading beam was connected to the end face of the horizontal jack by using the screw and the end plate. The rigid distribution beam was placed on the top of the specimen to evenly distribute the pressure of the jackshaft to the wall so that the stress state of the model was closer to the engineering practice. The roller was set between the vertical jack and the beam to ensure that the vertical jack could move with the lateral displacement of the specimen top.

The vertical load was first applied in the test, and the vertical load was applied to all the predetermined loads and remained constant during the trial. The horizontal loading process functions under the force-displacement dual control method. Specimens in the elastic phase following the force control are divided into three levels of loading, and each loading cycle is repeated one time; when the horizontal force-displacement curve of the top of the specimen shows an obvious turning point, the displacement control is used to load step-by-step. The displacement increment in each stage was 3 mm, and the load of each stage was cycled twice.

2.4. The Loading System and the Loading Procedure. The counter-force apparatus system is depicted in Figure 4, and all the specimens were fixed on the rigid floor through high-strength screws. The axial load was first applied to the models using a 1000 kN hydraulic jack, and it remained unchanged during the tests. The axial load applied on the two specimens was $0.2\,A_c f_c$ (f_c: average compressive strength of concrete; A_c: cross-sectional area of the wall). Because the

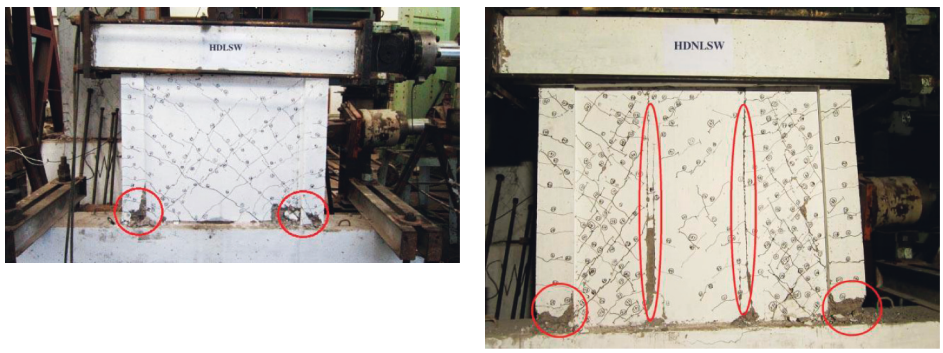

(a) (b)

Figure 6: Crack development of the two specimens: (a) specimen HDLSW; (b) specimen HDNLSW.

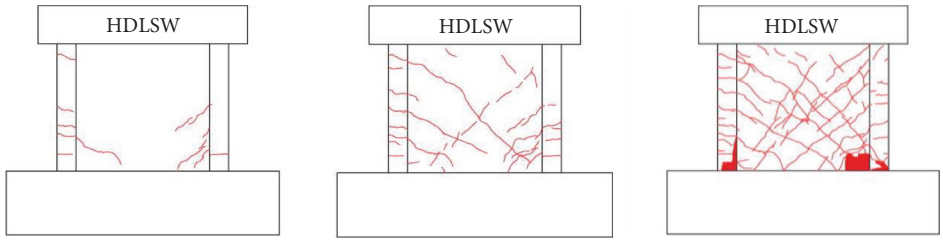

Figure 7: Crack development of the shear wall HDLSW.

hydraulic jack was installed on the frictionless rollers, the hydraulic jack could move freely in the lateral loading direction, and the free lateral displacement of the top end of the specimens appeared as a cantilever. A 1000 kN actuator provided the lateral loading. The quasi-static cyclic loading method was adopted for all specimens.

The lateral loading protocol for all specimens was under displacement control, as shown in Figure 5. Each loading cycle was repeated twice, and the experiments were stopped when the load dropped below 85% of the peak load [18].

2.5. Testing Contents. The physical quantities of each specimen were measured during the test, including the load, displacement, relative deformation, and strain. The displacement meter was set at the center of the loading beam to measure the vertex displacement of the tested piece. One horizontal displacement meter and two vertical displacement meters were arranged on the foundation beam to correct the influence of the translation and rotation of the foundation beam on the displacement value of the specimen. The vertical load was monitored frequently to control the specimen's axial compression ratio to keep it constant. In addition, several parallel concrete strain gauges are arranged at the lower part of the wallboard to study the plastic development of the shear wall.

3. Results and Analyses

3.1. Failure Process and Morphology of Specimens. The failure modes of each shear wall are shown in Figure 6. The failure modes of the two low-rise shear walls are entirely different. For the traditional low-rise shear wall HDLSW with concealed steel bracings, when the cracking load reaches, the horizontal cracks first appear at the bottom of the frame column and extend obliquely to the wallboard with an increase in the load. Upon further loading, multiple diagonal shear cracks appeared on the web and numerous horizontal cracks appeared on the frame column. As the load increased gradually, the original cracks extended and penetrated further, forming multiple shear oblique cracks through the web. The cracks intersect with each other into a mesh and divide the web into several small blocks. During the later loading period, the concrete at the corner of the web peeled off and the concrete at the bottom of the frame column was crushed. The failure mode of the component is mainly shear failure. The crack development diagram of the HDLSW shear wall is shown in Figure 7.

For the slotted low-rise shear wall HDNLSW, cracks first appeared along the two sides of the vertical slits. As the load increased, oblique cracks appeared on the web of the shear wall on both sides of the vertical slits and horizontal cracks appeared on the frame column. There was no crack in the built-in steel plate shear wall between the two vertical slits. With a further increase in the load, the shear walls on both sides of the vertical slits appeared as multiple cross oblique cracks and continued to extend; the frame columns on both sides appeared as multiple horizontal cracks, and oblique cracks began to appear on the middle web. During the later loading period, the shear walls on both sides of the vertical slits were filled with oblique cross cracks and the crack width increased significantly. The transverse reinforcement intersected with the oblique cracks yielded, and the concrete at the corner of the two frame columns was crushed. However, the shear wall between the two vertical slits maintained good integrity. The failure process of

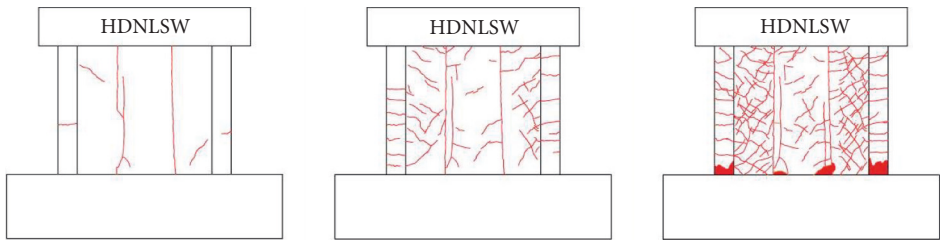

Figure 8: Crack development of the shear wall HDNLSW.

Table 3: Experimental results of bearing capacity of specimens.

Specimen	F_c/kN		F_y/kN		F_m/kN		μ_{cm} means	μ_{ym} means
	Positive	Negative	Positive	Negative	Positive	Negative	F_c/F_m	F_y/F_m
HDLSW	71.2	−72.8	308.5	−297.3	511.6	−503.8	0.14	0.60
HDNLSW	73.7	−70.1	318.6	−302.5	494.8	−480.1	0.15	0.64

Table 4: Experimental results of displacements and ductility coefficients of specimens.

Specimen	U_c/mm		U_y/mm		U_d/mm		μ means
	Positive	Negative	Positive	Negative	Positive	Negative	U_d/U_y
HDLSW	0.57	−0.56	8.31	−8.15	30.11	−29.85	3.64
HDNLSW	0.74	−0.70	9.71	−9.26	40.8	−39.48	4.23

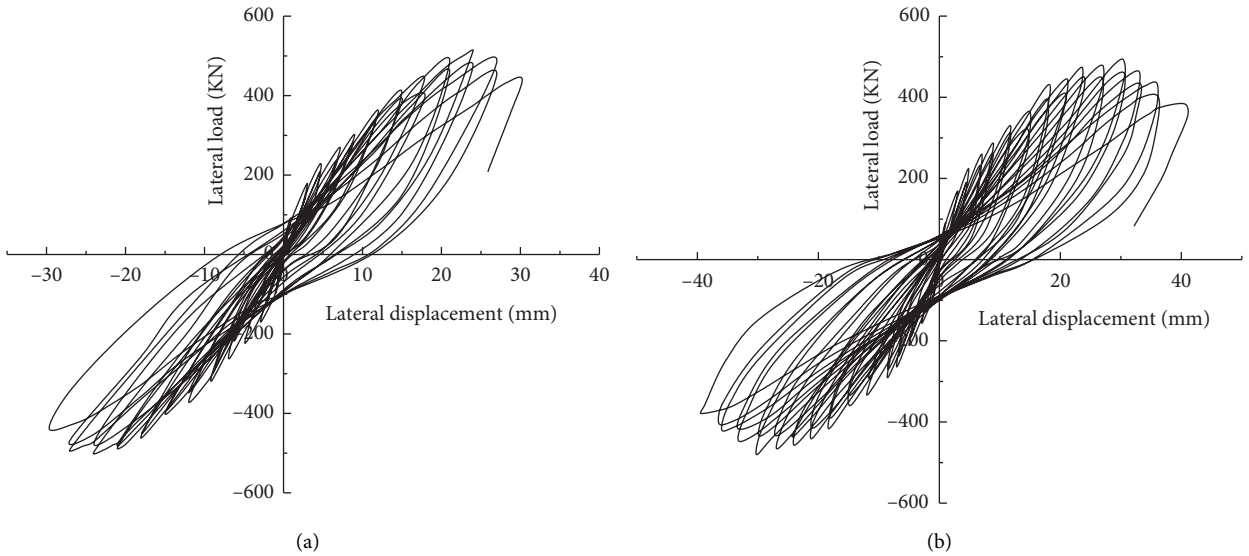

Figure 9: Lateral force versus the top displacement hysteretic curve. (a) HDLSW. (b) HDNLSW.

the shear wall shows good ductility. The crack development of the shear wall HDNLSW is shown in Figure 8.

3.2. Bearing Capacity and Ductility Analysis. Table 3 shows the measured values of the cracking, apparent yield, and ultimate loads of the two shear walls in this test. Table 4 shows the measured values of the top displacement and ductility coefficients of the two shear walls, in which F_c and U_c are the specimen's cracking load and cracking displacement, respectively, and the positive and negative mean values are obtained. F_y and U_y are the yield load and the yield displacement of the specimen, respectively, and their values are calculated using the equal energy principle. F_m is the maximum horizontal load of the specimen, U_d is the maximum elastic-plastic displacement value when the load does not decrease significantly, μ_{cm} is the ratio of the cracking load to the ultimate load, and μ_{ym} is the ratio of the yield load to the ultimate load.

Comparing the test results of the two shear walls, it can be seen that the cracking load and the yield load of the two shear walls are almost the same, but the bearing capacity of the shear wall HDNLSW decreases slightly (by 4%). At the same time, the ultimate displacement and the ductility ratio

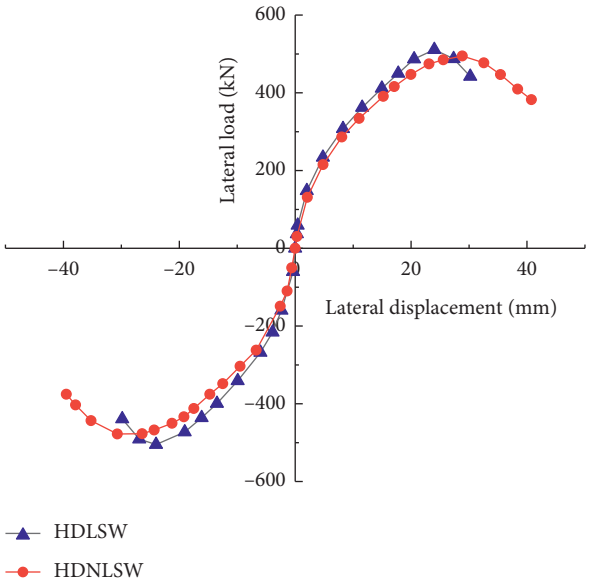

Figure 10: Force-displacement skeleton curves of two specimens.

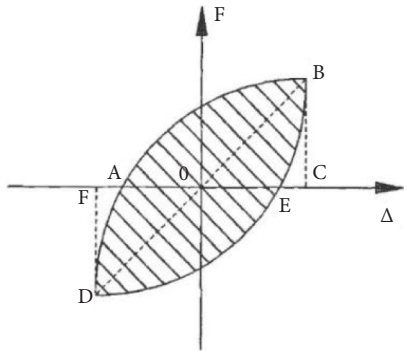

Figure 11: Calculation of the equivalent viscosity coefficient.

of the shear wall HDNLSW are also increased by 33.9% and 16.2%, respectively.

3.3. Hysteresis Characteristic Analysis and Skeleton Curve Comparison. The hysteretic curves and skeleton curves of the two shear walls are shown in Figures 9 and 10. The hysteresis curve can comprehensively reflect the shear wall strength, stiffness, deformation capacity, and energy dissipation capacity. It can be seen from Figure 9 that the hysteretic curve of HDNLSW is more plumped than that of HDLSW, indicating that the new shear wall has a better energy dissipation capacity. It can also be seen from the skeleton curve that the bearing capacity of the shear wall HDLSW decreases faster after reaching the peak load Although the maximum bearing capacity of the shear wall HDNLSW decreased slightly, the decrease in the bearing capacity was not evident after the peak load and the bearing capacity was relatively stable and had better deformation performance.

3.4. Energy Dissipation Capability Analysis. The equivalent viscous damping coefficient h_e and the area around the

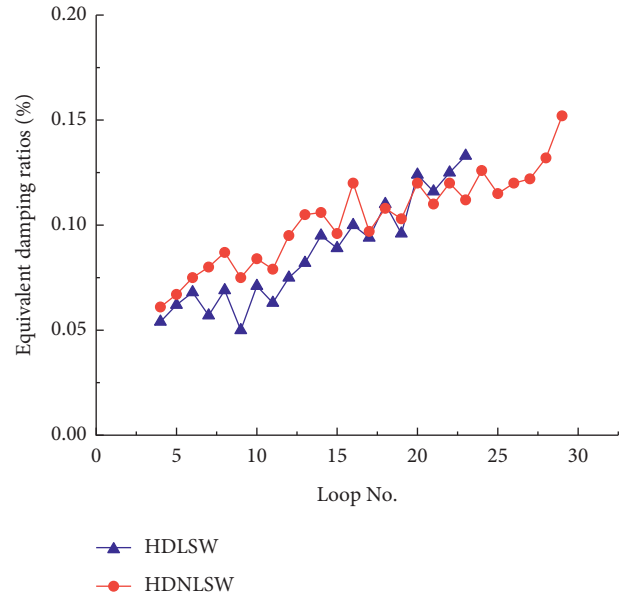

Figure 12: Equivalent viscous damping ratios of two specimens.

skeleton curve and the coordinate axis can be used as quantitative indexes to measure the energy dissipation capacity of the component. The equivalent viscous damping coefficient represents the fullness of the hysteresis curve of the structure. The calculation formula is shown in Figure 11. The equivalent viscous damping coefficient was calculated using the following equation. The area (ABE + EDA) represents the dissipation energy at each loading cycle, and the area (OBC + ODF) represents the elastic strain energy at each loading cycle, as depicted in Figure 11.

$$h_e = \frac{1}{2\pi} \frac{\text{Area}(\text{ABE} + \text{EDA})}{\text{Area}(\text{OBC} + \text{ODF})}. \quad (1)$$

The equivalent viscous damping coefficient-loading cycle curve is shown in Figure 12. It can be seen that the equivalent viscous damping coefficient increases with the increase in the number of cycles. Overall, the equivalent viscous damping coefficient h_e of the shear wall HDNLSW is greater than that of the low-rise shear wall HDLSW, indicating that the shear wall HDNLSW has good energy dissipation capacity.

The area enclosed by the skeleton curve and the coordinate axis reflects the total energy consumption of the component. The average calculation results of the area surrounded by each skeleton curve and coordinate axis were as follows: HDLSW energy consumption was 11267.5 kN mm, and HDNLSW energy consumption was 15107.4 kN mm. Therefore, the energy consumption of HDNLSW is 34.1%, which is higher than that of HDLSW.

3.5. Analysis of the Stiffness Degradation Process. The stiffness of the shear wall specimen is related to the stress level and the number of loading cycles. The stiffness is variable during loading. For the needs of seismic response analysis, the change in secant stiffness during loading is given in this

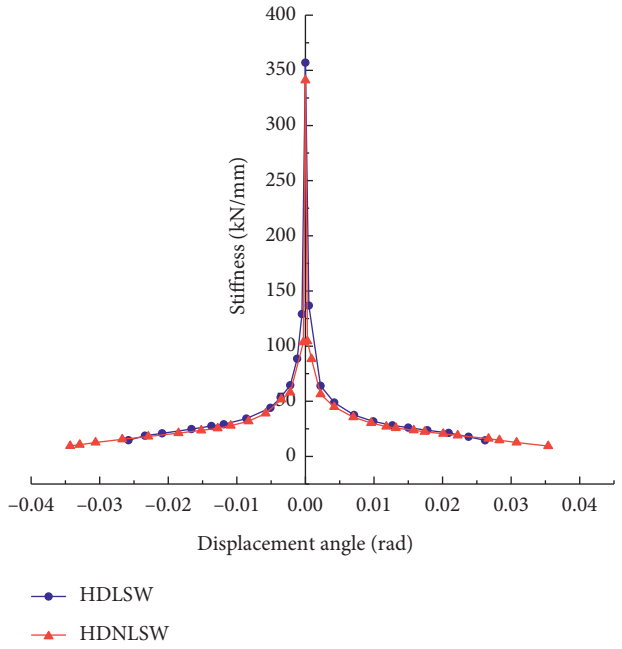

Figure 13: The contrast diagram of attenuation curves of rigidity.

Table 5: Variance of the frequency and the damping ratio of undamaged and damaged specimens.

Specimen	Before test		After test	
	Frequency/ Hz	Damping ratio/%	Frequency/ Hz	Damping ratio/%
HDLSW	175.4	3.2	82.6	9.4
HDNLSW	173.2	3.4	90.1	12.3

paper. The specific calculation formula for the secant stiffness is shown in the following formula(2):

$$K_i = \frac{|+F_i| + |-F_i|}{|+\Delta_i| + |-\Delta_i|}. \quad (2)$$

Here, $\pm Fi$ are the maximum positive and negative loads of the i^{th} loading cycle, respectively, and $\pm \Delta_i$ are the displacements corresponding to $\pm$ Fi. The stiffness degradation curves for the two specimens are shown in Figure 13.

Table 5 shows the stiffness at each stage of the two shear walls, where K_0 represents the initial stiffness, K_c represents the cracking stiffness, K_y represents the yield stiffness, β_{c0} represents the stiffness attenuation from the initial stage to the cracking stage, and β_{y0} represents the stiffness attenuation from the initial stage to the yield stage.

The initial stiffness K_0 (corresponding to the elastic stage), cracking stiffness K_c (corresponding to the cracking load), yield stiffness Ky (corresponding to the yield load), and the stiffness degradation coefficient β ($\beta_{y0} = K_y/K_0$, $\beta_{c0} = K_c/K_0$) of the two specimens are computed and are listed in Table 6.

It can be seen that the stiffness of the two shear walls is similar before cracking, indicating that the mortar bars in the HDNLSW vertical slits of the specimen at the beginning stage work together with the wall panels on both sides. After cracking, the stiffness of the HDNLSW decreased rapidly owing to the influence of the vertical slits and the cracking stiffness decreased by 21.6% compared with that of HDLSW. It is worth noting that the stiffness degradation of the HDNLSW shear wall in the early stage is greater than that of HDLSW. Still, the stiffness degradation in the late phase is slow, indicating that it has good residual stiffness, mainly because the built-in steel plate composite wallboard in the middle part maintains good integrity. Meanwhile, it can also be seen that the ultimate displacement angle of the shear wall HDNLSW is larger, indicating that the new low-rise shear wall is safer under severe earthquakes.

Table 6: Experimental results of stiffness of specimens.

Specimen	K_0 kN·mm^{-1}	K_c kN·mm^{-1}	K_y kN·mm^{-1}	B_{c0} K_c/K_0	β_{y0} K_y/K_0
HDLSW	357.2	127.46	36.80	0.36	0.10
HDNLSW	341.3	99.87	32.74	0.29	0.10

3.6. Damping Performance Analysis. The dynamic tests of the two shear walls before and after the tests were carried out using the free attenuation method, and the first-order frequency and the modal damping ratio of each shear wall were measured, as shown in Table 6. The test results show that there was little difference in frequency between the two shear walls before the test, indicating that the stiffness difference between them is small. After failure, the frequency of the shear wall HDNLSW was greater, indicating that its residual stiffness is larger, which was more conducive to structural earthquake resistance.

Damping reflects the attenuation of the vibration energy of an object. The damping ratio is the ratio of the damping force to the critical damping force, representing the damping force's magnitude. In the elastic stage, damping is mainly related to the material. The material and size of the two specimens were the same, so the damping ratios were similar. After the structure enters the plastic stage, damping is mainly related to structural damage. It can be seen that the new shear wall has a more excellent damping ratio after the test, implying that it has a better energy dissipation capacity. This is because the cracks between the mortar strip and the wallboard on both sides increase the friction energy consumption of the wallboard under a reciprocating load, thus improving the structural damping.

4. Discussion

In order to solve the problem of poor deformation capacity of a conventional low-rise shear wall, a new shear wall with an embedded steel plate and vertical slits was proposed in this paper. Through the comparative test of the two shear walls, it can be seen that the function of two vertical slits was to change the original low-rise shear wall into three high-rise shear walls. Thus, the brittle failure of the original low-rise

shear wall was transformed into ductile failure. At the same time, the embedded steel plate can improve the stiffness and bearing capacity of the shear wall with vertical slits and reduce the weakening effect of slit treatment on the low-rise shear wall. This finding provides a basis for the optimized design of shear walls.

This study only completed a comparative test of the two shear walls to verify the rationality of the new shear wall. However, the theoretical calculation and reasonable parameters of the new shear wall, such as the location of the crack and the size of the built-in steel plate, need to be studied further. The next step will be to establish a numerical model for verification and further for the mechanical procedure and parameter analysis.

5. Conclusion

The following findings can be obtained from the experimental research and analysis of two distinct kinds of shear walls:

(1) Compared with the traditional concealed bracing low-rise shear wall, the deformation capacity and energy dissipation capacity of the new low-rise shear wall are significantly improved and they have a good bearing capacity. The hysteresis loop was more plumped, and the seismic performance was better.

(2) The traditional low-rise shear wall with concealed bracing is mainly brittle shear failure. In contrast, the new low-rise shear wall exhibits bending loss with good ductility, and the failure is primarily concentrated on the two sides of the vertical slits of the shear wall. The shear wall between the vertical slits was slightly damaged, and the failure mode was more reasonable. Because the shear wall between the vertical slits still has a high bearing capacity after the failure of the shear wall on both sides of the vertical slits, a clear two-way seismic defense line is formed, which can meet the requirements of no collapse under strong earthquakes.

(3) The new low-rise shear wall can meet different mechanical properties. By adjusting the width of the shear wall between the vertical slits and the size of the steel plate, shear walls with varying capacities of bearing and ductility can be obtained to meet different needs. However, further studies are required for a proper seam position and an economical steel plate size.

Data Availability

The data used to support the findings of this study are available from the corresponding author upon request.

Conflicts of Interest

The authors declare that there are no conflicts of interest.

Acknowledgments

This paper was supported by the Ministry of Housing and Urban-Rural Development of China Research Project (No. 2017-K9-010) and the Science and Technology Program of Yangzhou (YZ2019138).

References

[1] C. R. Farrar, J. W. Reed, and M. W. Salmon, "Failure modes of low-rise shear walls," *Journal of Energy Engineering*, vol. 119, no. 2, pp. 119–138, 1993.

[2] T. N. Salonikios, A. J. Kappos, I. A. Tegos, and G. G. Penelis, "Cyclic load behavior of low-slenderness RC walls:failure modes, strength, and deformation analysis, and design implications," *ACI Structural Journal*, vol. 97, no. 1, pp. 132–141, 2000.

[3] W. Y. Kam, S. Pampanin, and K. Elwood, "Seismic performance of reinforced concrete buildings in the 22 February Christchurch (Lyttelton) earthquake," *Bulletin of the New Zealand Society for Earthquake Engineering*, vol. 44, no. 4, pp. 239–278, 2011.

[4] K. Muto, *Structural Dynamic Design*, pp. 87–90, China Architecture and Building Press, Beijing, 1984.

[5] H. J. Jiang, X. L. Lu, and Y. K. Cheung, "Study on a seismic slit shear wall with cyclic experiment and macro-model analysis," *Structural Engineering & Mechanics*, vol. 16, no. 4, pp. 371–390, 2003.

[6] X. L. Lu, X. L. Dang, J. Qian, Y. Zhou, and H. J. Jiang, "Experimental study of self-centering shear walls with horizontal bottom slits," *Journal of Structural Engineering*, vol. 143, no. 3, 2017.

[7] C. Sittipunt, S. L. Wood, and P. Lukkunaprasit, "Cyclic behavior of reinforced concrete structural walls with diagonal web reinforcement," *ACI Structural Joural*, vol. 98, no. 4, p. 554, 2001.

[8] S. Shaingchin, P. Lukkunaprasit, and S. L. Wood, "Influence of diagonal web reinforcement on cyclic behavior of structural walls," *Engineering Structures*, vol. 29, no. 4, pp. 498–510, 2007.

[9] J. W. Zhang, W. L. Cao, C. Yu, and H. Y. Dong, "Shake table test of reinforced concrete wall structure with concealed bracings," *Proceedings of the Institution of Civil Engineers - Structures and Buildings*, vol. 167, no. 10, pp. 598–609, 2014.

[10] D. Zhang, Z. Tao, and L. Zhang, "Research on deformation behavior of reinforced concrete composite shear wall with concealed bracings based on performamce," *Engineering Rview*, vol. 37, no. 2, pp. 111–121, 2017.

[11] M. Gan, M. Kang, C. Long, and L. R. Li, "Cyclic response of scaled low-rise shear walls with concealed bracings," *Materiali in tehnologije*, vol. 54, no. 4, pp. 447–455, 2020.

[12] W. Wang, Y. Z. Ren, Z. Lu, K. L. Song, and Y. Zhou, "Experimental study of the hysteretic behaviour of corrugated steel plate shear walls and steel plate reinforced concrete composite shear walls," *Journal of Constructional Steel Research*, vol. 160, pp. 136–152, 2019.

[13] W. Wang, Y. Wang, and Z. Lu, "Experimental study on seismic behavior of steel plate reinforced concrete composite shear wall," *Engineering Structures*, vol. 160, pp. 281–292, 2018.

[14] D. Dan, A. Fabian, and V. Stoian, "Nonlinear behavior of composite shear walls with vertical steel encased profiles," *Engineering Structures*, vol. 33, no. 10, pp. 2794–2804, 2011.

[15] C. J. Gan and L. V. Xilin, "Computational simulation of nonlinearity of steel plate reinforced concrete shear walls," *Journal of Structural Engineering*, vol. 30, no. 5, pp. 97–102, 2009.
[16] Z. Zhou, J. Qian, and W. Huang, "Numerical study on deformation capacity of steel plate reinforced concrete shear walls," *Advances in Civil Engineering*, vol. 34, 2019.
[17] *Code for Design of concrete Structures: GB 50010-2010*, China Architecture & Building Press, Beijing, 2015.
[18] *Specification for Seismic Test of Buildings: JGJ/T 101-2015*, China Architecture & Building Press, Beijing, 2015.